Applied Physics Letters ARTICLE scitation.org/journal/apl

Multiple phase transitions in Sc doped Sb_2Te_3 amorphous nanocomposites under high pressure

Cite as: Appl. Phys. Lett. **116**, 021903 (2020); doi: 10.1063/1.5131489
Submitted: 15 October 2019 · Accepted: 26 December 2019 ·
Published Online: 14 January 2020

Teng Zhang,[1,2] Kai Zhang,[2,a)] Gang Wang,[1,b)] Eran Greenberg,[3] Vitali B. Prakapenka,[3] and Wenge Yang[2,c)]

AFFILIATIONS

[1]Laboratory for Microstructures, Institute of Materials, Shanghai University, Shanghai 200444, China
[2]Center for High Pressure Science and Technology Advanced Research (HPSTAR), 1690 Cailun Road, Pudong, Shanghai 201203, China
[3]Center for Advanced Radiation Sources, University of Chicago, Chicago, Illinois 60637, USA

[a)]E-mail: kai.zhang@hpstar.ac.cn
[b)]E-mail: g.wang@shu.edu.cn
[c)]E-mail: yangwg@hpstar.ac.cn

ABSTRACT

Subnanosecond switching speed from an amorphous state with stable crystal precursors to the crystalline state was recently achieved in amorphous Sc-doped Sb_2Te_3 (a-SST) phase change materials (PCMs), which is about two orders of magnitude faster than that in the well-studied $Ge_2Sb_2Te_5$ and $Ge_1Sb_2Te_4$ PCMs. However, the phase change mechanism and phase stability of a-SST remain unknown. Here, we prepared amorphous $Sc_{0.3}Sb_2Te_3$ nanocomposites within a minute amount of face-centered-cubic (FCC) type nanograins embedded in the amorphous matrix. Using *in situ* high-pressure synchrotron X-ray diffraction, we found that nanograins were frustrated under high pressure and gradually dissolved into the matrix around 11.0 GPa. Beyond 11.0 GPa, the a-SST matrix transformed into a uniform high density metallic like amorphous state with a five orders of magnitude drop in electric resistivity compared to the pristine materials. When further compressed to 23.97 GPa, the high density amorphous (HDA) phase switched into a body-centered-cubic (BCC) high-pressure structure, a different phase from the ambient pressure crystalline structure. Upon decompression back to ambient pressure, a pure amorphous phase was sustained. The present study provides additional insight into the phase change mechanism of amorphous nanocomposites.

Phase-change random access memory (PCRAM) is regarded as the leading candidate for the next-generation electronic storage industry.[1] The biggest challenge is the development of phase change material (PCM), which greatly determines the writing speed of commercialized PCRAM products. A critical characteristic of PCM for memory applications is its ultrafast, reversible phase transformation between amorphous and crystalline states, which utilized pronounced electric resistance contrast between two states. Realizing improved trade-off between crystallization speed (writing) and amorphous phase stability (data retention) remains a challenging issue in PCM. Over the past few decades, amorphous $Ge_2Sb_2Te_5$ and $Ge_1Sb_2Te_4$ (both referred to as GST in this Letter) have received much attention as the matured PCMs,[2–7] but are still limited by the tens of nanoseconds writing speed due to the stochastic crystal nucleation during crystallization. Prototypical amorphous Sb_2Te_3 shows a more rapid crystallization rate than GST at high temperature but has poor thermal stability at room temperature.[8] Numerous methods have been proposed to develop more advanced types of PCMs, including the doping method, preannealing, etc.[9–11]

Recently, the alloying strategy was projected by doping transition metals into the Sb_2Te_3 host compound, which aimed to form geometrically conformable crystal precursors with cubic Sb_2Te_3 in the as-synthesized amorphous state. Rao *et al.* screened Sc as a valid dopant to achieve subnanosecond high-speed cache-memory in amorphous $Sc_{0.2}Sb_2Te_3$.[1] Similar memory behaviors were further verified in Sc-doped GST[9] and Sc-doped Sb_2Te[12] phase change memory alloys. The *ab initio* study demonstrated that subnanosecond writing speed (crystallization) stemmed from reduced stochasticity of nucleation through geometrically matched and robust Sc-Te square motifs that stabilized crystal precursors in the amorphous phase. It should be noted that the chemical environment in amorphous Sc-doped Sb_2Te_3 (a-SST) can be largely altered by just low-doped Sc.[13] The sensitive response of the structural feature to the chemical composition naturally raised the question about the structural stability of a-SST. Related

temperature or pressure-driven phase transitions have been widely discussed in amorphous GST PCM.[3,14] The high-pressure technique has been proved to be an efficient method to tailor the structure and property of PCM,[15] especially for the chalcogenide PCMs that contain significant amounts of vacancies[16,17] that are very sensitive to external pressure.[15,18,19] For example, GST showed diverse phase change behaviors between amorphous and crystalline states when subjected to high pressure. With the help of *in situ* high-pressure X-ray diffraction, we can probe the fine structural information during the phase transition process. Phase change behavior in amorphous nanocomposites under high pressure has so far been scarce, which not only involves the stability of nanocrystals under high pressure but also the mutual interaction mechanism between the nanocrystal and the amorphous matrix. Meanwhile, one may argue whether a pre-existing nanocrystalline precursor could facilitate the phase transition under high pressure, which remains unexplored.

The a-SST samples were prepared by magnetron cosputtering of pure Sc and Sb_2Te_3 targets onto a glass substrate at room temperature in an Ar atmosphere. The film composition was determined by using an energy dispersive spectrometer (EDS). The composition of a-SST in this work is determined to be $Sc_{0.3}Sb_2Te_3$ (5.6 at. % Sc doping). The film was scraped off the substrate for X-ray diffraction and Raman and electric resistance measurements under high pressure. Silicone oil was used as the pressure transmitting medium. The high-pressure X-ray diffraction (XRD) measurements were carried out by using a diamond anvil cell (DAC) at the 13-IDD station ($\lambda = 0.2952$ Å), Advanced Photon Source (APS), Argonne National Laboratory. The pressure was calibrated using the equation of state of Au and ruby fluorescence method. The 633 nm excitation emerging from the He-Ne laser was used to record the Raman spectra with an incident laser power of 3.4 mW and a data collection time of 10 mins. For the electric resistance measurement, a setup of four-probe measurement configuration is depicted in the inset in Fig. 4.

To probe the phase stability of a-SST nanocomposites, *in situ* high-pressure X-ray diffraction was conducted during the compression and decompression cycle at room temperature up to ~40.89 GPa, as shown in Fig. 1. At 0.78 GPa, the XRD pattern shows an amorphous profile but with several weak diffraction peaks, marked by the black arrows in Fig. 1(a), which indicates that some small grains exist in the as-deposited amorphous phase. Meanwhile, as shown by the green curve at the bottom of Fig. 1(a), the crystalline SST diffraction pattern with a face-centered-cubic (FCC) structure at 0.82 GPa is also plotted for comparison with a-SST. It is easily identified that the small diffraction peaks lying in the amorphous phase are derived from the FCC type nanocrystal phase. Under high pressure, a-SST remained in the amorphous state up to ~21.89 GPa. Upon compression, all peaks shifted to the higher diffraction angle side, which demonstrated gradual volume compression for amorphous and nanocrystalline phases. A clear change was also reflected in structure factors S(q) as shown in Fig. S1. When the pressure is further increased to ~23.97 GPa, an abrupt crystallization is observed as shown in Fig. 1(b). The XRD pattern can be nicely matched to a body-centered-cubic (BCC) phase, as shown in Fig. S2. SST remained in the BCC phase up to 40.89 GPa, and upon decompression, BCC transformed back to the amorphous phase, which can be retained at ambient pressure.

The pair distribution function g(r) provides real-space structural information that can be deduced from scattering intensities.[20] As

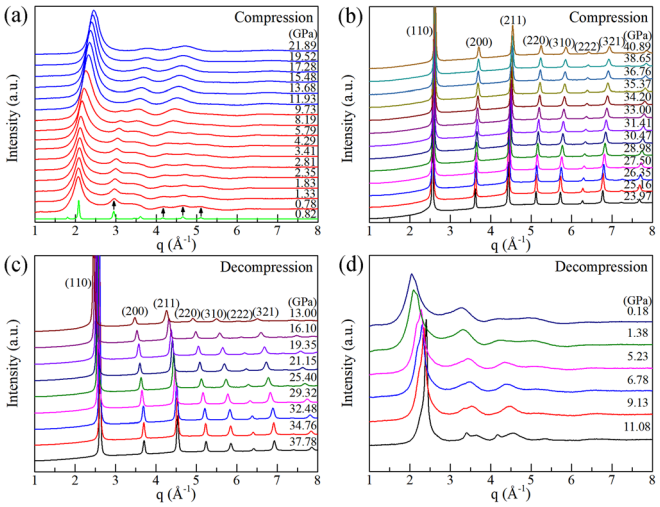

FIG. 1. *In situ* XRD spectra of the a-SST sample under hydrostatic pressure. Note the gradual disappearance of nanocrystals up to 11.93 GPa (a) and from amorphous to BCC-SST at ~23.97 GPa (b), upon subsequent decompression, the high pressure BCC phase stays (c) until it returns to the amorphous state at ~11.08 GPa, and this amorphous phase can be retained to ambient pressure (d).

shown in Fig. 2(a), r_1, r_2, r_3, and r_4 peaks correspond to distances of different coordination shells, respectively. At the initial pressure, the r_1 and r_2 peaks are distinctly separated. With increasing pressure, the r_2 peak gradually became weak and turned into a shoulder of the r_1 peak at about 11.93 GPa, which implied the atomic rearrangement in a local structure. The systematic *ab initio* study of the relevant parent compounds Sc_2Te_3 and Sb_2Te_3 has been performed in Ref. 13. With regard to the g(r) calculated based on the *ab initio* molecular dynamics (AIMD) trajectories, the r_1 peaks for Sb-Te, Sc-Te, and Sb-Sb bonds are located around 2.93 Å and the r_2 peaks for Sb-Sb, Te-Te, and Sb-Te are found at 4.14 Å. Strong second-nearest-neighbor Te-Te, Sb-Sb interactions play an important role in the connection of octahedral or defective octahedral units, which results in the formation of a covalent network.[21] This interaction can even determine the long-range order of the metastable cubic phase of GST.[18] With increasing pressure, the r_2 peak gradually shifts to the left, which showed that atomic correlation at distance r_2 was weaken, and the r_1 peak became highly asymmetric. At 0.78 GPa, the majority of Sc and Sb atoms are sixfold and fourfold coordinated.[13] The r_1 peak is mainly derived from the Sb-Te and Sb-Sb bonds and a small amount of Sc-Te bonds due to the low doping of Sc. It is well known that the coordination number (CN) can directly reflect the number of atoms around a central atom. CN of a-SST is shown in Fig. 2(b), which is obtained by multiplying the half-integral of the first shell of the radial distribution function (RDF) curve by two. It can be found that at initial pressure, CN of a-SST is around 5.1, i.e., the average of six-coordinated Sc and four-coordinated Sb. When the volume is compressed, the r_2 peak gradually shifts to the left and merges into the r_1 peak. The materials transformed from low density amorphous (LDA) to high density amorphous (HDA). The correlations of the Te-Te bond and Sb-Sb bond around 4 Å are weakened, and the correlations around 3 Å are increased, causing Sc and Sb atoms to reach a higher coordination state. Finally, CN reached 7.5 at about 11.0 GPa. After 11.0 GPa, CN roughly remained at 7.5 that has

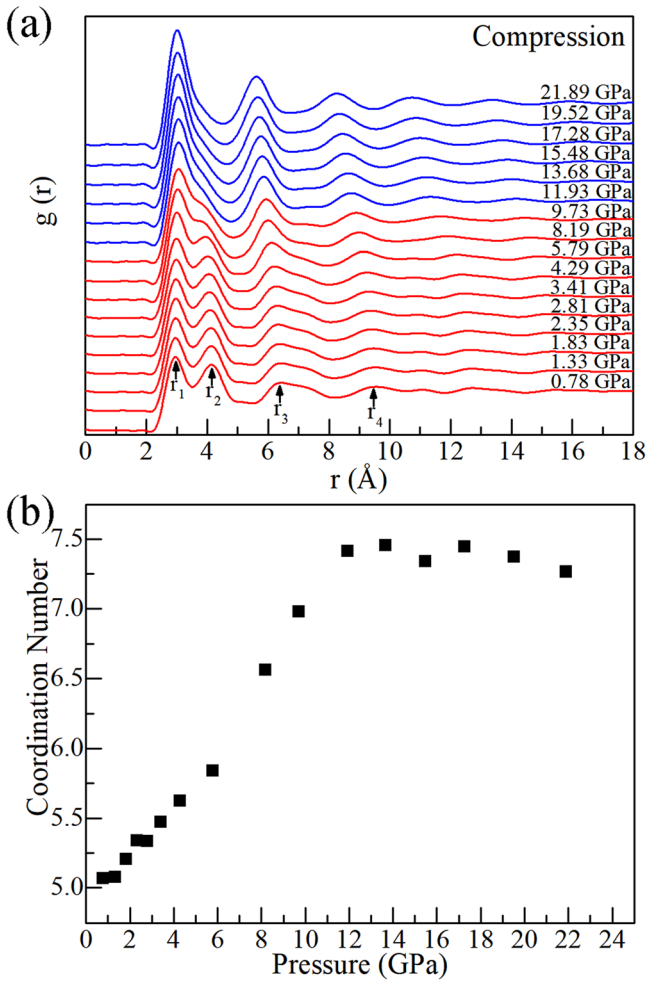

FIG. 2. (a) Evolution of the pair distribution function g(r) as a function of pressure. (b) The coordination number of a-SST with applied pressure.

been very close to the eight-coordinated high-pressure BCC structure. Therefore, upon further compression, the HDA abruptly transforms into a BCC phase.

The detailed evolutions of the position of peaks in g(r) are shown in Fig. 3. As the volume is compressed, the distance between atoms normally decreases, as shown in Figs. 3(a) and 3(b). The positions of the r_2, r_3, and r_4 peaks shift toward a smaller r value with increasing pressure, whereas the position of r_1, which is related to the bond length in the nearest interatomic distance, does not shorten but shows a small expansion in spite of volume contraction as indicated in Fig. 3(a). The bond length expands up to 11 GPa, saturates, and then shortens after 11 GPa. This abnormal bond expansion-contraction behavior was attributed to pressure-induced suppression of the Peierls distortion[22,23] as found in liquid GeX (X = S, Se and Te). It is caused by the alternate strong Sb-Te bond and weak Sb-Sb bond in a-SST. The ensemble of features indicated a possible amorphous-amorphous transition in a-SST at high pressure.

Phase change memory mainly utilizes the distinct resistance difference between amorphous and crystalline states. To understand the phase-change mechanism of a-SST, we performed high-pressure resistance measurements. As depicted in Fig. 4, the room temperature resistance of a-SST drops sharply by more than five orders of magnitude from the initial pressure to 11.0 GPa, which corresponds to a potential pressure-induced amorphous-amorphous transition, as also indicated in the XRD patterns. Finally, the resistance decreases slowly and remains roughly constant. This behavior is in accordance with the pressure-induced phase change in amorphous GST.[6,7] Finally, upon decompression, the resistance returns to the initial value. This distinct physical property originated from different bonding mechanisms in amorphous and crystalline phases. The principle of Raman effect is based on the inelastic light-scattering process between incident photons and the phonons in materials,[24] which enables probing of local vibrational modes of SST and therefore offers an effective method for monitoring the evolution of atomic structures during pressure-induced phase transition. Raman spectra of a-SST under high pressure were measured as shown in Fig. S3, which shows a similar phase transition sequence to the structure and electrical resistance measurements. Upon

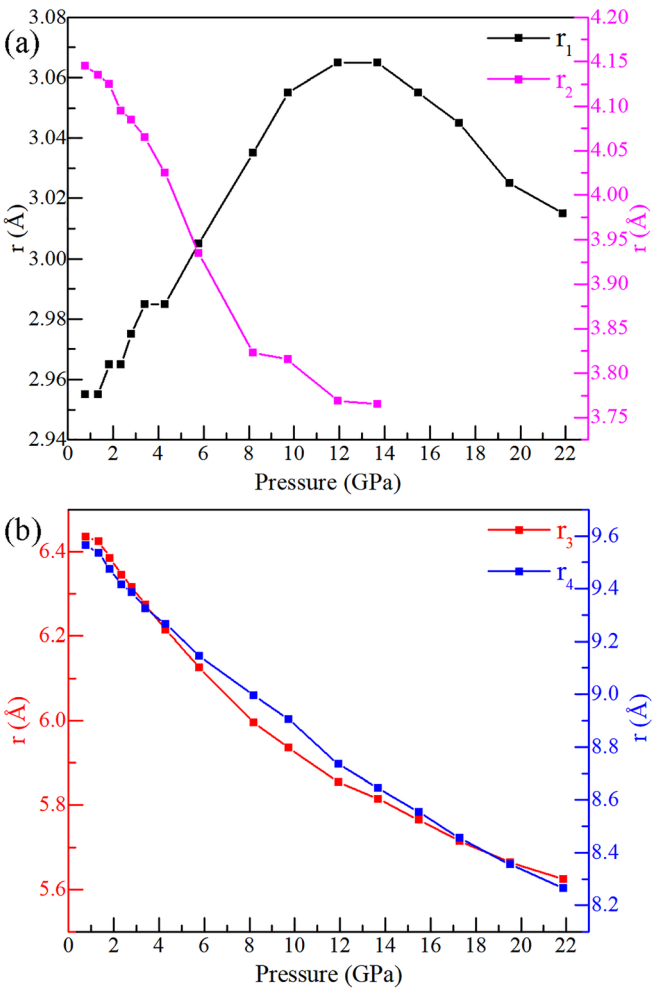

FIG. 3. (a) and (b) The pressure dependence for the position of the first, the second, the third, and the fourth peaks in g(r).

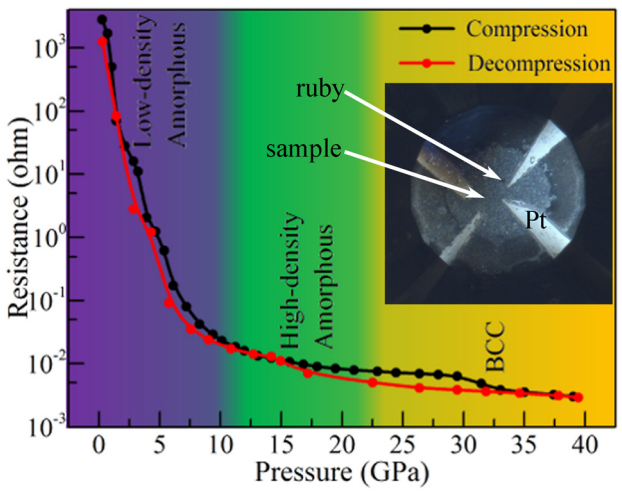

FIG. 4. Room temperature resistance under pressure. Resistance as a function of pressure of a-SST during loading and unloading processes. Shadow regions in different colors indicate different phases. The inset shows the contact configuration of four platinum probes under pressure.

decompression, the Raman character reappeared. The combined XRD, Raman, and resistance measurements indicated that a pressure-induced transition between LDA semiconducting and HDA metallic forms of a-SST occurred at $P \sim 11$ GPa.

It should be noted that LDA-HDA transition of the amorphous matrix and disappearance of nanocrystals are concomitant from the initial pressure to 11 GPa. Bulk FCC-SST has an even richer atomic vacancy (1/6) than GST (1/10), which is prone to disordering under high pressure[1,18] by the displacement of Te atoms filling the neighboring vacancies.[25] Therefore, when subjected to high pressure, FCC type nanocrystals will gradually destabilize to form the amorphous phase and further dissolve into the amorphous matrix. The mismatch of compressibility between the amorphous matrix and the nanocrystal gives rise to nonuniform strain distribution at the interface, which, in return, promotes the disappearance of nanocrystals. This case is in accord with the GST system in which c-GST has a higher bulk modulus than a-GST at low pressure.[25] As a consequence of the evolution of nanocrystals, the amorphous matrix showed an abnormally increased full-width at half-maximum (FWHM) before 11 GPa, as shown in Fig. S4, which implied the formation of a more disordered amorphous phase. This is in contrast to normal pressure-induced ordering in pure a-GST.[3] During the practical phase change process, stress is ubiquitous at the phase interface due to the volume difference between crystalline and amorphous phases.[26] Therefore, our work provides additional insight into the structural evolution of PCM.

In summary, a-SST shows a highly similar structural evolution behavior to a-GST under high pressure. We have observed that the as-deposited a-SST has pre-existing nanocrystals that can be nicely indexed to the FCC type crystal by the Bragg equation. As the pressure increases, nanocrystals do not directly facilitate the formation of a high-pressure BCC phase, but disappear around 11.0 GPa, where the original a-SST transforms to a more disordered amorphous phase. Then, HDA crystallizes into a BCC structure phase at about 23.0 GPa. BCC-SST is retained during the unloading process until 11.0 GPa, before it transforms back to the amorphous state. The large hysteresis loop suggests pronounced kinetic constraints on the phase change under pressure.

See the supplementary material for structure factors S(q) of a-SST in the pressure range of 0–21.89 GPa before crystallization (Fig. S1), Rietveld refinement of the BCC-SST at 23.97 GPa at the first crystalline pressure point (Fig. S2), Raman spectra of a-SST in compression and decompression cycles (Fig. S3), evolution of full-width at half-maximum (FWHM) of the first peak in a-SST XRD in the pressure range of 0–21.89 GPa (Fig. S4), and the analysis procedure of the amorphous diffraction data.

Part of this research was carried out at the Extreme Conditions Beamline (P02.2) at DESY, a member of Helmholtz Association (HGF). We are very thankful to Konstantin Glazyrin for the technical support. This work was supported by the National Natural Science Foundation of China under Grants Nos. 11804010, U1530402, and 51527801 and China Postdoctoral Science Foundation (Grant No. 2016M600909). The beamline 13-ID-D (GeoSoilEnviroCARS) was supported by the National Science Foundation (NSF)—Earth Sciences (No. EAR-1128799)—and Department of Energy (DOE)—GeoSciences (No. DE-FG02-94ER14466). APS was supported by DOE-BES, under Contract No. DE-AC02-06CH11357.

REFERENCES

[1]F. Rao, K. Y. Ding, Y. X. Zhou, Y. H. Zheng, M. J. Xia, S. L. Lv, Z. T. Song, S. L. Feng, I. Ronneberger, R. Mazzarello, W. Zhang, and E. Ma, Science **358**, 1423 (2017).
[2]Y. Q. Cheng, M. Xu, H. W. Sheng, Y. Meng, X. D. Han, and E. Ma, Appl. Phys. Lett. **95**, 131904 (2009).
[3]M. Xu, Y. Meng, Y. Q. Cheng, H. W. Sheng, X. D. Han, and E. Ma, J. Appl. Phys. **108**, 083519 (2010).
[4]M. Krbal, A. V. Kolobov, J. Haines, A. Pradel, M. Ribes, P. Fons, J. Tominaga, C. Levelut, R. L. Parc, and M. Hanfland, Appl. Phys. Lett. **93**, 031918 (2008).
[5]Z. M. Sun, J. Zhou, Y. C. Pan, Z. T. Song, H. K. Mao, and R. Ahuja, Proc. Natl. Acad. Sci. U. S. A. **108**, 10410 (2011).
[6]B. Hen, S. Layek, M. Goldstein, V. Shelukhin, M. Karpovski, E. Greenberg, E. Sterer, Y. Dagan, G. K. Rozenberg, and A. Palevski, Phys. Rev. B **97**, 024513 (2018).
[7]E. Greenberg, B. Hen, S. Layek, I. Pozin, R. Friedman, V. Rosenberg, M. Karpovski, M. P. Pasternak, E. Sterer, Y. Dagan, G. K. Rozenberg, and A. Palevski, Phys. Rev. B **95**, 064514 (2017).
[8]R. Jeyasingh, S. W. Fong, J. Lee, Z. Li, K. W. Chang, D. Mantegazza, M. Asheghi, K. E. Goodson, and H. S. P. Wong, Nano Lett. **14**, 3419 (2014).
[9]Y. Wang, Y. H. Zheng, G. Y. Liu, T. Li, T. Q. Guo, Y. Cheng, S. L. Lv, S. N. Song, K. Ren, and Z. T. Song, Appl. Phys. Lett. **112**, 133104 (2018).
[10]K. L. Xu, X. S. Miao, and M. Xu, Phys. Status Solidi RRL **13**, 1800506 (2019).
[11]D. Loke, T. H. Lee, W. J. Wang, L. P. Shi, R. Zhao, Y. C. Yeo, T. C. Chong, and S. R. Elliott, Science **336**, 1566 (2012).
[12]X. Chen, Y. H. Zheng, M. Zhu, K. Ren, Y. Wang, T. Li, G. Y. Liu, T. Q. Guo, L. Wu, X. Q. Liu, Y. Cheng, and Z. T. Song, Sci. Rep. **8**, 6839 (2018).
[13]G. M. Zewdie, Y. X. Zhou, L. Sun, F. Rao, V. L. Deringer, R. Mazzarello, and W. Zhang, Chem. Mater. **31**, 4008 (2019).
[14]T. Siegrist, P. Jost, H. Volker, M. Woda, P. Merkelbach, C. Schlockermann, and M. Wuttig, Nat. Mater. **10**, 202 (2011).
[15]M. Xu, Y. Q. Cheng, L. Wang, H. W. Sheng, Y. Meng, W. G. Yang, X. D. Han, and E. Ma, Proc. Natl. Acad. Sci. U. S. A. **109**, E1055 (2012).
[16]W. Zhang, A. Thiess, P. Zalden, R. Zeller, P. H. Dederichs, J. Y. Raty, M. Wuttig, S. Blügel, and R. Mazzarello, Nat. Mater. **11**, 952 (2012).
[17]Z. M. Sun, J. Zhou, A. Blomqvist, B. Johansson, and R. Ahuja, Phys. Rev. Lett. **102**, 075504 (2009).

[18]A. V. Kolobov, J. Haines, A. Pradel, M. Rides, P. Fons, J. Tominaga, Y. Katayama, T. Hammouda, and T. Uruga, Phys. Rev. Lett. **97**, 035701 (2006).
[19]A. V. Kolobov, J. Haines, A. Pradel, M. Rides, P. Fons, J. Tominaga, C. Steimer, G. Aquilanti, and S. Pascarelli, Appl. Phys. Lett. **91**, 021911 (2007).
[20]M. Tomomasa, T. Higaki, T. Hayakawa, A. Chiba, and K. Tsuji, J. Phys.: Conf. Ser. **121**, 022007 (2008).
[21]A. Hirata, T. Ichitsubo, P. F. Guan, T. Fujita, and M. W. Chen, Phys. Rev. Lett. **120**, 205502 (2018).
[22]J. Nakamura, A. Chiba, and K. Tsuji, J. Phys. Soc. Jpn. **79**, 064604 (2010).
[23]A. Chiba, M. Tomomasa, T. Hayakawa, S. M. Bennington, A. C. Hannon, and K. Tsuji, Phys. Rev. B **80**, 060201 (2009).
[24]A. F. Goncharov, Int. J. Spectrosc. **2012**, 1.
[25]S. Caravati, M. Bernasconi, T. D. Kuhne, M. Krack, and M. Parrinello, Phys. Rev. Lett. **102**, 205502 (2009).
[26]O. M. Roscioni, P. S. Branicio, J. Kalikka, X. Zhou, and R. E. Simpson, Appl. Phys. Lett. **112**, 151901 (2018).